# PROGRESS IN THREE-DIMENSIONAL SIMULATIONS OF EXPLOSIONS AND EARTHQUAKES

Arthur J. Rodgers, Oleg Vorobiev, N. Anders Petersson, Bjorn A. Sjogreen, and William Foxall

Lawrence Livermore National Laboratory

Sponsored by the National Nuclear Security Administration

Award No. DE-AC52-07NA27344/LL09-Simulation-NDD02

## ABSTRACT

We report results of simulations of explosion- and earthquake-generated wave propagation in three-dimensional (3D) earth models. Computer codes at Lawrence Livermore National Laboratory (LLNL) model the nonlinear (hydrodynamic) and linear (anelastic) response of the earth to arbitrary forcing with material properties varying in 3D. In order to simulate the ranges and frequencies of interest to nuclear explosion monitoring, we run simulations on massively parallel computers at LLNL, often on hundreds or thousands of CPUs. Simulations broadly cover three thrust areas: (1) nonlinear shock-wave (hydrodynamic) modeling of explosions; (2) near-field elastic modeling of explosions, including free-surface topography; and (3) regional-scale modeling of earthquakes and explosions. Hydrodynamic simulations are performed with GEODYN, an Eulerian finite volume code for modeling shock-waves in earth materials. Local and near-regional scale elastic simulations are performed with WPP, a Cartesian finite difference code for seismic wave modeling. Regional simulations are performed with SPECFEM_3D_GLOBE, a code based upon the spectral element method in spherical geometry. These capabilities are joined for modeling explosion ground motions to local distances with a one-way coupling to pass hydrodynamic motions from GEODYN to WPP. We continue to improve these capabilities to support nuclear explosion monitoring research, for example, to study special events and/or understand specific phenomena of seismic sources and wave propagation.

In the last year, we have made progress in each thrust. We have worked to facilitate hydrodynamic modeling and pass motions from GEODYN to WPP. We are modeling the HUMBLE REDWOOD series of explosions in order to validate material models and one-way coupling of GEODYN to WPP. We have done extensive calculations of the effect of free-surface topography on shallow explosions. We show that shear waves can be very effectively generated by P-to-S scattering by surface topography, and the P-coda and Rg wave spectra are shaped by the source spectrum. Regional simulations of earthquakes near the North Korean nuclear test site show that 3D models can predict the waveforms at near-regional distances. The 2009 nuclear test can be modeled with a pure explosion plus a small double-couple (10% $M_0$ of the explosion) composed of strike-slip mechanisms, consistent with nearby earthquakes.

## OBJECTIVES

Advances in numerical methods for modeling seismic wave excitation and propagation and ever more powerful parallel computers are making it easier to simulate ground motions on the scale lengths (domain sizes) and frequencies (resolutions) of importance to nuclear explosion monitoring. The objective of this research is to develop and improve methods for seismic simulation in fully 3D earth models to improve nuclear explosion monitoring. Specifically, research is directed along three thrusts: modeling of shock-wave propagation with hydrodynamic methods; modeling of elastic propagation near shallow explosions and earthquakes, including the effect of 3D volumetric structure and free-surface topography; and regional broadband waveform modeling. This effort relies on numerical methods for 3D wave phenomena implemented in computer codes running on massively parallel computers. These capabilities allow us to investigate source and propagation phenomenology of explosion sources and understand waveform data from specific events of interest.

## RESEARCH ACCOMPLISHED

In the following sections we describe research accomplished on several tasks.

### Modeling the HUMBLE REDWOOD Explosions

We performed preliminary modeling of the HUMBLE REDWOOD series of explosions. These explosions were conducted above and below the ground surface and were recorded by seismic (ground motion) and acoustic (air blast) sensors (Foxall et al., 2010). The purpose of this experiment was to develop methods for yield estimation of explosions that are not fully contained and require joint consideration of the amplitudes of the air blast and seismic waves. We are working on coupled modeling of the explosive source with GEODYN (to simulate the shock wave in solid earth and the air above) with motions subsequently passed to WPP for seismic wave propagation, as described in Rodgers et al. (2009). The preliminary modeling shown here is for one of the contained explosions (5 m depth of burial) and was performed to evaluate how well purely elastic modeling and a preliminary seismic model predict the recorded response.

Figure 1a shows the experimental configuration, with the explosion shot points and recording stations for weak motions (velocity sensors). The experiments involved strong motion (accelerometer) and air-blast (acoustic) sensors as well, but we do consider those data in this study. Figure 1b shows the preliminary model for shear wave speeds. The orientation of the basement was determined from seismic refraction data. We maintained this geometry of alluvium-basement interface, modified the velocities, and compared the simulated ground motions with the recorded ground motions. Modeling was done with an isotropic (explosion) buried source and purely elastic propagation.

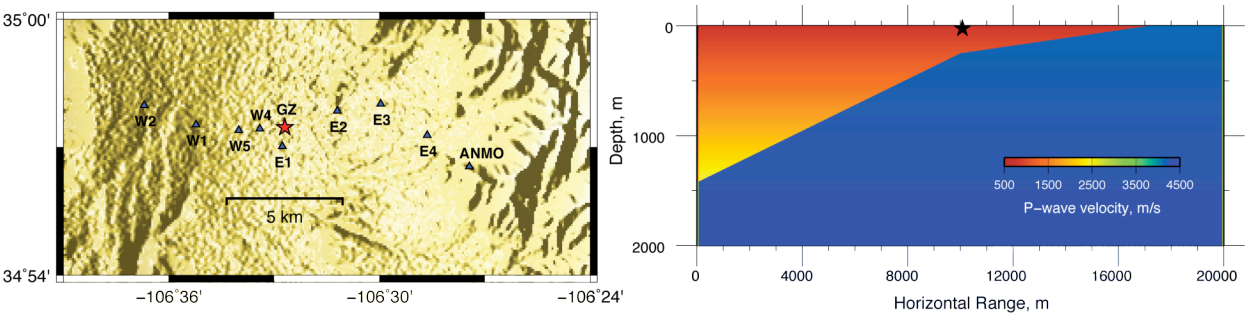


**Figure 1. (a) Map of the HUMBLE REDWOOD experiment, with shot points and seismic weak motions recording stations (triangles) overlain on surface topography. (b) Vertical cross section of the preliminary velocity model showing the P-wave speeds. In both panels the star indicates the shot point.**

Figure 2 shows the comparison of the recorded (blue) and simulated (red) vertical component, ground velocity time histories for shot HR1-G (5 m depth of burial). The recorded and simulated ground motions were filtered 0.3–1.0 Hz. The shot occurred over a change in the dip of the basement, thus the near-surface structure is quite different between the east and west. These differences are apparent in the recorded motions, which show different

arrival times (note group velocity indications) and a simpler response for the western stations, composed of a P- and S-wave (Rg), and for the eastern stations, which show a very long duration surface wave. The surface wave to the eastern stations appears to be attenuated relative to the simulated response. Attenuation was not included in the simulations; however, not surprisingly it appears to be important for propagation in the alluvium. At higher frequencies the model fit becomes worse, suggesting that the source model, as well as attenuation, needs to be considered. The model could certainly be improved to predict the arrival times, dispersions, and amplitudes.

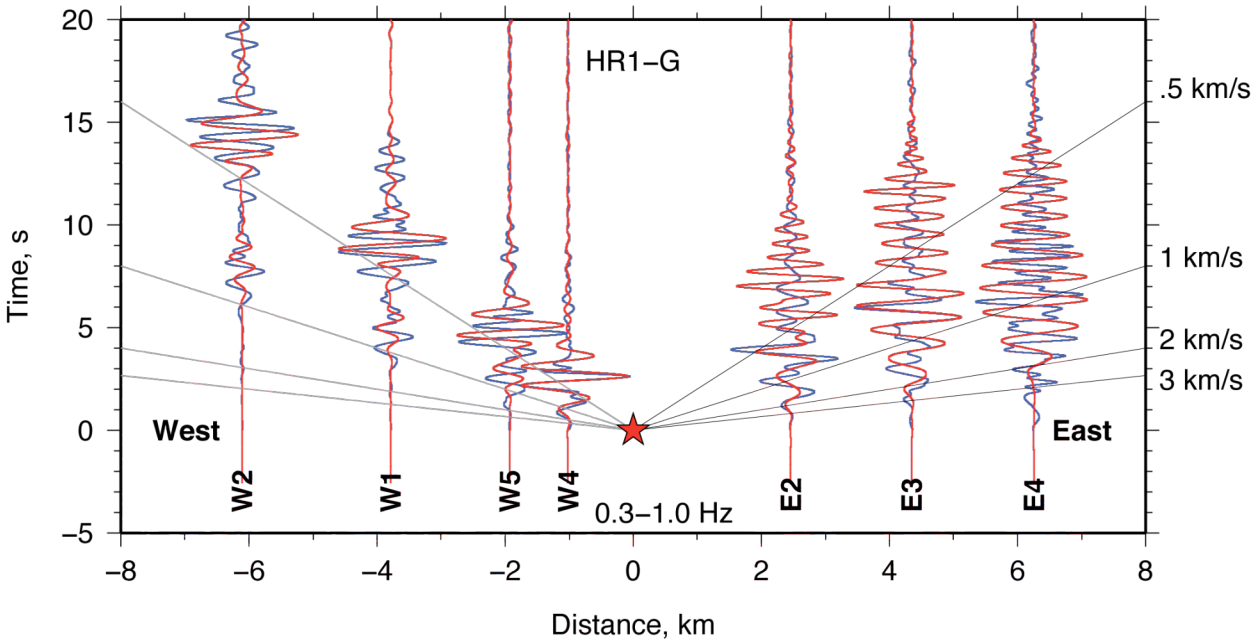


**Figure 2. Comparison of observed (blue) and synthetic (red) vertical component ground velocity time histories for HUMBLE REDWOOD shot HR1-G, plotted as record section. The data and synthetics are filtered between 0.3–1 Hz. Gray lines indicate the 3-, 2-, 1-, and 0.5-km/s group velocities in both directions.**

### Topographic Scattering and Shear-Wave Generation Near Shallow Explosions

In the last year simulations were performed of the 2006 and 2009 North Korean nuclear tests, using reported locations and including the effect of free-surface topography on wavefield (Rodgers, 2010; Rodgers et al., 2010a,b). We modeled the near-field response for a domain covering 40 km around the source. Simulations were performed at high resolution (up to 8 Hz) to capture the frequencies of interest for regional high-frequency discrimination and yield estimation. Figure 3 shows the study area, surface topography, and reported locations of the explosions.

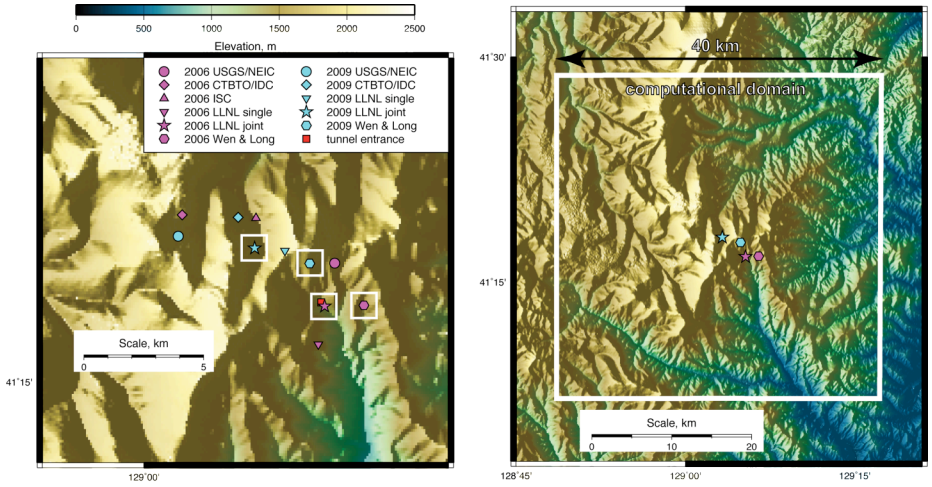


**Figure 3. (left) Reported locations of 2006 (magenta) and 2009 (cyan) North Korean nuclear tests. (right) Computational domain for elastic simulations, including free-surface topography (color scale).**

The simulations used a homogeneous half-space model but included the actual free-surface topography from the Shuttle Radar Topography Mission, with 90-meter resolution (Farr et al., 2007). The inclusion of rough free-surface topography has a strong effect on the ground motion. Figure 4a shows an image of the vertical component velocities for the flat and topographic cases, using the LLNL location of the 2009 event. The flat response is very simple, with outward-propagating P and Rg waves. Notice that the topographic case shows strong azimuthal variations before the waves have traveled more than 3 km (1 s). A strong distortion in the wavefield is caused by the steep slope to the southwest of the shot point, and this results in a large-amplitude Rg at later times and farther distances (indicated by the arrow in Figure 4a). At longer times the topographic response shows strong scattering of P-to-Rg energy. Much of the energy between P and Rg travels with the Rg velocity.

When the same source (isotropic moment tensor, depth of 600 m) is used, but at four different locations, the response can be quite different. Figure 4b shows the vertical-component ground-velocity responses for four different locations: LLNL and Wen and Long (2010) for the 2006 and 2009 events. This indicates that the response is strongly impacted by the topography. In further analysis we showed that the amplitudes of downward-propagating waves can be affected with focusing and defocusing by topographic features, causing variations of a factor of 2 or more and leading to an effective asymmetric radiation pattern (Rodgers et al., 2010b).

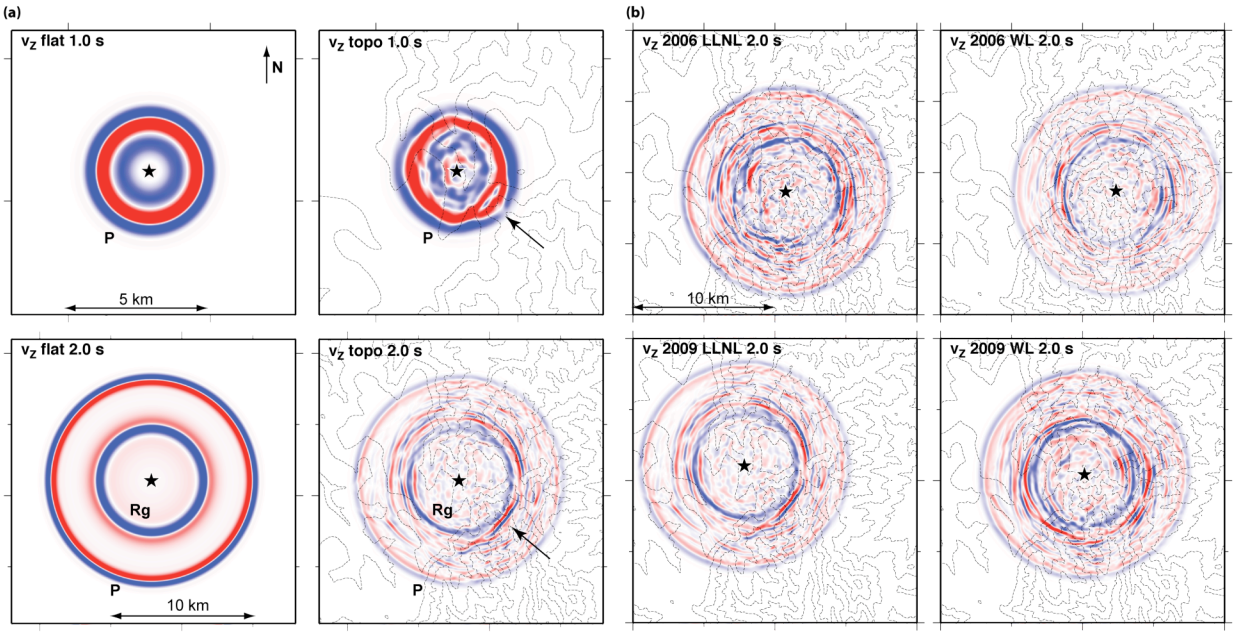


**Figure 4. (a) Vertical-component ground velocity at two time steps (1 and 2 s, note different scales) for the flat (left) and topographic (right) cases, assuming the LLNL location of the 2009 event. (b) Vertical-component ground velocity at 2 s after the event for four different locations, LLNL and WL (Wen and Long, 2010), for the 2006 and 2009 events.**

Variability in the wave field seen in Figure 2 is clear in the ground-motion time histories as well. Figure 5 shows the three-component ground velocities for the vertical, radial, and transverse components recorded at 10 km for two filter bands 0.5–2 Hz and 2–8 Hz. For reference, the motions for the flat case are also shown. Note that below 2 Hz the topographic response is similar to the flat case, but above 2 Hz topographic scattering causes significant complexity in the wave field, particularly the P-wave coda (between P and Rg) and Rg. Also note that above 2 Hz the transverse component response can have amplitudes equal to that on the vertical and radial component. Note that the ground velocities plotted in full-field view in Figure 4 and as time histories in Figure 5 show higher-frequency response for the topographic cases than for the flat case, especially the Rg phase. P-to-S scattering by topography tends to capture high-frequency energy from the source and propagate it along the surface.

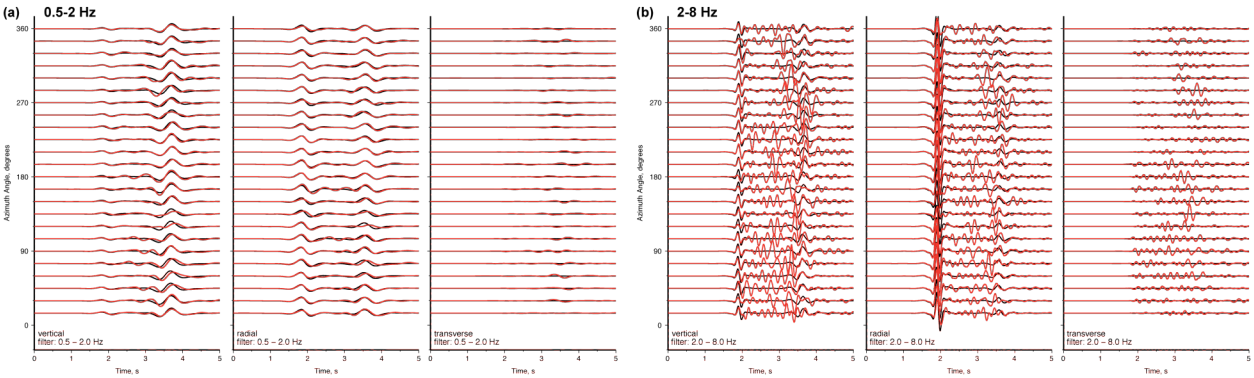


**Figure 5. Ground-velocity time histories on the surface at 10 km as a function of azimuth filtered (a) 0.5–2 Hz and (b) 2–8 Hz for the vertical (left), radial (center), and transverse (right) components. The responses are plotted for the flat (black) and topographic (red) cases with the same amplitude scale for all three components and both filter bands.**

In order to further understand the simulated response, we measured the spectral amplitudes of carefully windowed segments of the wavefield for the flat and topographic case. Figure 6a shows such an example, where the P, P-coda (energy between the P and Rg phases), and Rg phases are indicated by the color-coded windows for the flat and topographic cases. The Fourier spectral amplitudes are plotted in Figure 6b. Note that the P-wave spectra are nearly identical, with the topographic case slightly lower than the flat case. The P-wave coda in the topographic case is composed of P-to-P and P-to-Rg scattered energy and has a similar spectrum as the direct P-wave with modulation caused by path-specific scattering, while the amplitude of the P-wave coda for the flat case is very small in both the time and frequency domains. The Rg phase in the flat case is peaked at about 1.5 Hz and falls off very quickly with increasing frequency. However, in the topographic case, the Rg phase has the low-frequency spectral amplitude of the Rg in the flat case (i.e., peaked between 1–2 Hz) plus the high-frequency spectral amplitudes of the P-wave. These spectral measurements show how the Rg waves in the topographic case have the low-frequency spectral characteristics of the Rg phase for the flat earth and high-frequency spectral characteristics of the P-wave. P-coda waves have the spectral characteristics of the direct P-wave. Scattering of P-to-Rg can increase amplitudes of regional S-wave, particularly Lg, and will require further study to understand the propagation mode of this enhanced S-wave energy from explosion sources.

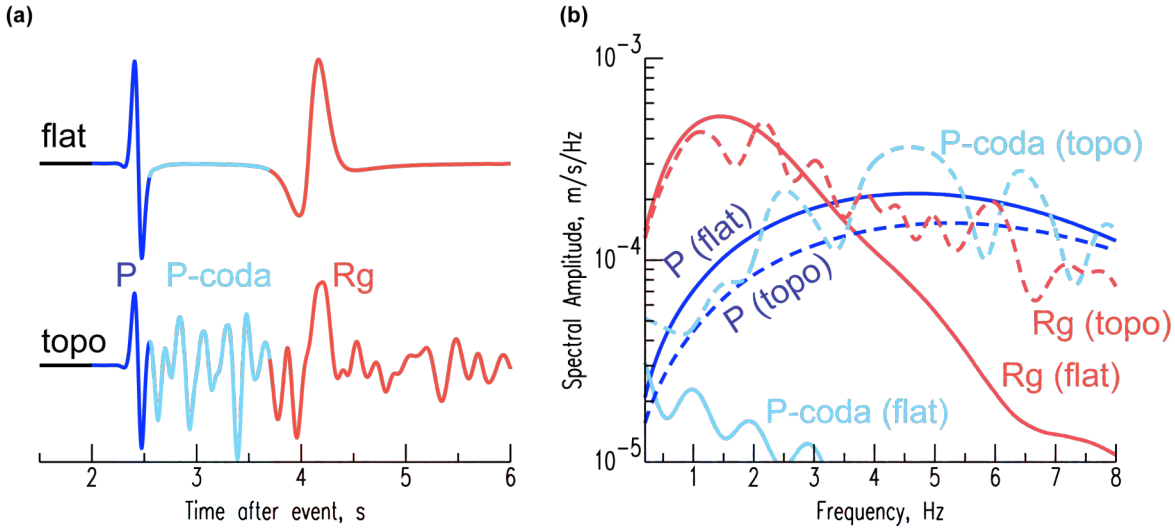


**Figure 6. (a) Vertical-component velocity time series for the flat (top) and topographic (bottom) cases, with the direct P (blue), P-wave coda composed of scattered energy (cyan) and Rg (magenta). (b) The Fourier amplitude spectra for the six colored waveform segments shown in (a) for the flat (solid lines) and topographic (dashed lines) cases. Note that the P-coda spectrum for the topographic case is similar to the direct P-wave, and the Rg spectrum for the topographic case is composed of the Rg spectra from the flat case for low frequencies plus the P-wave spectrum for high frequencies.**

### Regional Waveform Modeling and a Double-Couple Component from the 2009 North Korean Nuclear Test

We modeled the 2006 and 2009 North Korean nuclear tests and nearby earthquakes using the 3D *s29ea* (Kustowski et al., 2008) models. Calculations were made with SPECFEM3D_GLOBE, the spherical geometry spectral element method (Komatitsch and Tromp, 1999) code distributed by the Computational Infrastructure for Geodynamics (CIG, 2010). Figure 7a shows a map of the events and stations used in this analysis. Double-couple focal mechanisms for the regional earthquakes were estimated with the Cut-and-Paste method (Zhao and Helmberger, 1994; Zhu and Helmberger, 1996), which is based on a grid search using Green's functions from a plane-layered (one-dimensional, [1D]) model. Using the double-couple solutions for the earthquakes, we computed the response at regional stations. Figure 7b shows the fits to broadband waveform using the 3D *s29ea* model and our estimated source parameters for the two earthquakes at two stations (MDJ to the north and TJN to the south). Data and synthetics were filtered 0.02–0.07 Hz (14–50 s periods) and are plotted in absolute time and amplitude. Note that the waveforms are well fit

in this frequency band. This provides validation of the 3D seismic model and confidence that we can predict waveforms in this frequency band.

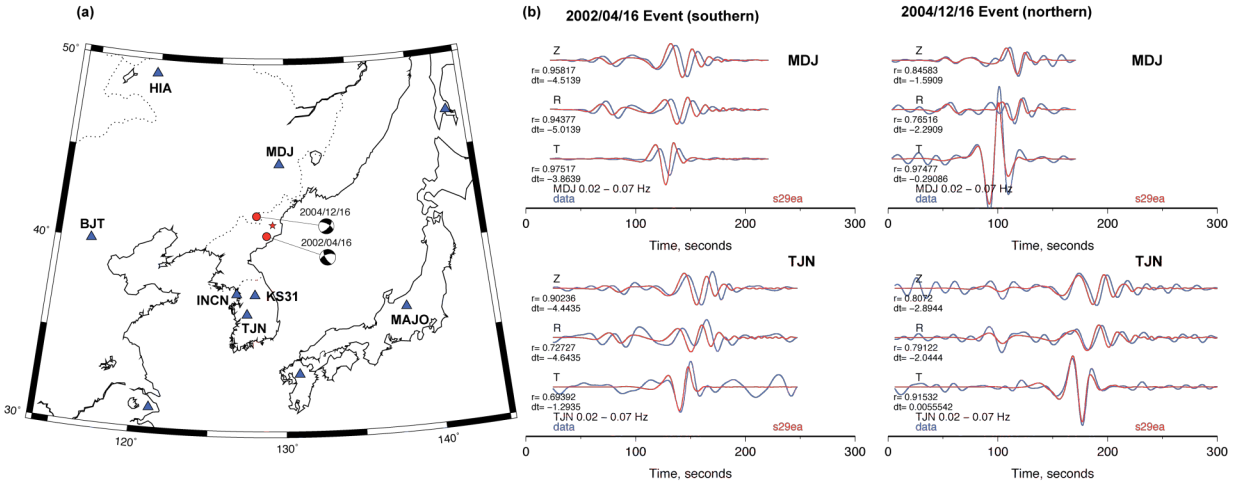


**Figure 7. (a) Map showing the locations of the North Korean nuclear tests (stars) and nearby earthquakes (circles) and focal mechanisms, along with regional broadband stations (triangles). (b) Waveform fits for the two earthquakes at stations MDJ and TJN. Data (blue) and synthetics (red) were filtered 0.02-0.07 Hz and are plotted in absolute time and amplitude.**

When the same 3D model is used to predict the waveforms from the larger May 25, 2009, North Korean nuclear test and the isotropic source model reported by Ford et al. (2009), we obtain good fits to the vertical and radial components (Figure 8a). Note, however, that the transverse components show an apparent Love wave not predicted by the source model or path propagation in the 3D. Analysis of the particle motion (not shown) at several regional stations indicates that the Love wave precedes the Rayleigh wave. We used the residual waveforms from the purely isotropic source to estimate a double-couple focal mechanism. This is reduced to estimating the source from the Love waves, which is highly nonunique due to the slow variation of the Love wave radiation pattern with azimuth. However, if the mechanism is constrained to be steeply dipping, we obtain a solution that is very consistent with the strike-slip mechanisms of the nearby earthquakes and does not degrade the fit to the Rayleigh waves on the vertical and radial components (Figure 8b). The source of the Love waves from the 2009 explosion is likely to be coincident in time and space with the explosion (isotropic) source and could be due to tectonic release or damage in the source zone (e.g., Ben-Zion and Ampuero, 2009).

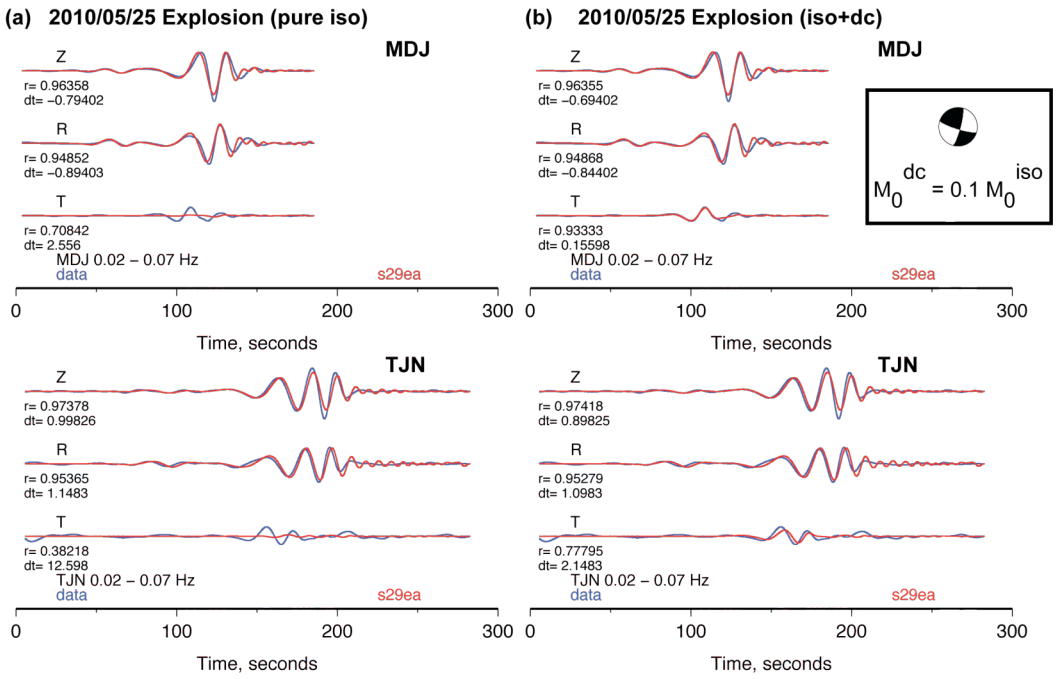


**Figure 8. Waveform fits for the 2010/05/25 explosion at stations MDJ and TJN for (a) pure isotropic source and (b) isotropic and 10% double-couple source with the focal mechanism shown. Data (blue) and synthetics (red) were filtered 0.02–0.07 Hz and are plotted in absolute time and amplitude.**

## CONCLUSIONS AND RECOMMENDATIONS

We continue to make progress on numerical modeling of seismic ground motions to improve nuclear explosion monitoring. Advances in mathematical methods to represent the physics of shock- and seismic-wave excitation and propagation enhance our efforts. Over the last year we have performed studies on small explosions to model the near-field response (HUMBLE REDWOOD); shallow explosions in the presence of rough surface topography to understand how topography impacts the response (North Korean nuclear test site); and regional-scale (400–1000 km), long-period (14–50 s) earthquakes and nuclear explosions in North Korea to improve source estimates.

## ACKNOWLEDGEMENTS

Arthur Rodgers is grateful for support as a Fulbright Scholar from the Council for International Exchange of Scholars and the Commission franco-américaine d'échanges universitaires et culture, to Michel Campillo for hosting him at the Laboratoire Géophysique Interne et Tectonophysique Université Joseph Fourier, Grenoble, France, and to LLNL for granting professional research and teaching leave. The authors thank Jeff Wagoner for assistance with topographic data from the Shuttle Radar Topography Mission project. We are grateful to the LLNL Laboratory Directed Research and Development program for support to develop the WPP code. The WPP code is open source and available with documentation from the LLNL website (Petersson, 2010). Spectral element calculations were made with SPECFEM3D_GLOBE, which is developed, maintained, and distributed by CIG. Simulations were performed on parallel computers operated by Livermore Computing using a Grand Challenge Allocation. Waveform data were obtained from the Incorporated Research Institutions for Seismology's Data Management System (IRIS-DMC) and organized in the LLNL Seismic Research Database by Stan Ruppert and Terri Hauk. Waveforms were extracted from the database and prepared for waveform modeling using dbtool, developed by Eric Matzel. Figures were made with the Generic Mapping Tool (GMT, Wessel and Smith, 1998). Seismogram plots were made with pssac2, developed by Lupei Zhu and Brian Savage. We are also grateful to Stephen Myers for communications about vertical-component ground-velocity responses from the LLNL location, shown in Figure 4a,b.

## REFERENCES

Ben-Zion, Y. and J.-P. Ampuero (2009). Seismic radiation from regions sustaining material damage, *Geophys. J. Int.* 178: 1351–1356.

Computational Infrastructure for Geodynamics (2010). SPECFEM3D_GLOBE, www.geodynamics.org, accessed January 2010.

Farr, T. G., P. A. Rosen, E. Caro, R. Crippen, R. Duren, S. Hensley, M. Kobrick, M. Paller, E. Rodriguez, L. Roth, D. Seal, S. Shaffer, J. Shimada, J. Umland, M. Werner, M. Oskin, D. Burbank, and D. Alsdorf (2007). The Shuttle Radar Topography Mission, *Rev. Geophys.* 45: RG2004, doi:10.1029/2005RG000183.

Ford, S., D. Dreger, and W. Walter (2009). Source analysis of the Memorial Day explosion, Kimchaek, North Korean, *Geophys. Res. Lett.* 36: L21304, doi:10.1029/2009GL040003.

Foxall, B., R. Marrs, E. Lenox, R. Reinke, D. Seastrand, J. Bonner, K. Mayeda, and C. Snelson (2010). The HUMBLE REDWOOD seismic/acoustic coupling experiments: Joint inversion for yield using seismic, acoustic and crater data, *Seismo. Res. Lett.* 8: 315.

Komatitsch, D. and J. Tromp (1999). Introduction to the spectral-element method for 3-D seismic wave propagation, *Geophys. J. Int.* 139: 806–822.

Kustowski, B., G. Ekstrom, and A. Dziewonski (2008). The shear-wave velocity structure in the upper mantle beneath Eurasia, *Geophys. J. Int.* 174: 978–992, 10.1111/j.1365-246X.2008.03865.x.

Petersson, N. A. (2010). https://computation.llnl.gov/casc/serpentine/software.html (website).

Rodgers, A., O. Vorobiev, N. A. Petersson, and B. Sjogreen (2009). Simulation of seismic waves from underground explosions in geologic media, FY2009 progress report, Lawrence Livermore National Laboratory report LLNL-TR 420208

Rodgers, A. (2010). Simulation of seismic waves for nuclear explosion monitoring, Lawrence Livermore National Laboratory abstract, LLNL-ABS-422488, European Geophysical Union Annual Meeting, May 2–7, 2010, Vienna, Austria (submitted).

Rodgers, A., N. A. Petersson, and B. Sjogreen (2010a). Seismic simulations of recent DPRK nuclear explosions including the effects of free surface topography and 3D structure, abstract, Seismological Society of America Annual Meeting, April 20–23, 2010, Portland, OR, USA (submitted).

Rodgers, A., N. A. Petersson, and B. Sjogreen (2010b). Efficient generation of shear waves from shallow explosions by topographic scattering near the North Korean nuclear test site, *J. Geophys. Res.*(submitted).

Wen, L. and H. Long (2010). High-precision location of North Korea's 2009 nuclear test, *Seismo. Res. Lett.* 81: 26–29.

Wessel, P. and W. H. F. Smith (1998). New, improved version of Generic Mapping Tools released, *EOS Trans. Amer. Geophys. U.* 79: 579.

Zhao, L. S. and D. V. Helmberger (1994). Source estimation from broadband regional seismograms, *Bull. Seismo. Soc. Amer.* 84: 91–10.

Zhu, L. and D. V. Helmberger (1996a). Advancements in source estimation techniques using broadband regional seismograms, *Bull. Seismo. Soc. Amer.* 86: 1634–1641.